GEM-MACH-PAH (rev2488): a new high-resolution chemistry transport model for North American PAHs and benzene

Cynthia H. Whaley, Elisabeth Galarneau, Paul A. Makar, Ayodeji Akingunola, Wanmin Gong, Sylvie Gravel, Michael D. Moran, Craig Stroud, Junhua Zhang, and Qiong Zheng

SUPPLEMENTAL MATERIAL

CONTENTS

A: Table of measurement sites

Table A.1: Benzene and PAH network measurement sites in the Pam Am model domain. Note that NATTS documentation provides site IDs, but not names, therefore the first column provides the state where the particular site resides, and cities/towns were manually looked up and added for those sites that have PAH measurements.

Site name or State	Site ID	Latitude	Longitude	measurement
IADN sites				
University of Toronto, ON	UOT	43.8725	-79.18833	PAH wet dep
St Clair, ON	STC	42.53594	-82.38978	PAH wet dep
Burlington, ON	BUR	43.36889	-79.87028	PAH wet dep
Burnt Island, ON	BNT	45.82833	-82.94806	PAHs
Point Petre, ON	PPT	43.84278	-77.15361	PAHs/PAH wet dep
Sturgeon Point, NY	STP	42.69306	-79.055	PAHs/PAH wet dep
Cleveland, OH	CLV	41.49214	-81.67853	PAHs/PAH wet dep
Sleeping Bear Dunes, MI	SBD	44.76111	-86.0586	PAHs
Chicago IIT, IL	IIT	41.83444	-87.6247	PAHs
NAPS sites				
College and South, Windsor, ON	60211	42.29289	-83.0731	PAHs, benzene
Gage Institute, Toronto, ON	60427	43.65822	-79.3972	PAHs, benzene
Etobicoke South (Toronto Kipling), ON	60435	43.61076	-79.5219	PAHs, benzene
Elgin and Kelly, Hamilton, ON	60512	43.25778	-79.8617	PAHs, benzene
Experimental Farm, Simcoe, ON	62601	42.8569	-80.2703	PAHs, benzene
Egbert, ON	64401	44.23111	-79.7831	PAHs, benzene
Point Petre, ON	64601	43.84278	-77.1536	PAHs, benzene
Burnt Island, ON	65501	45.82833	-82.9481	PAHs, benzene
NATTS sites				
Middletown, OH	390170003	39.4938	-84.3543	benzene
OH	390350038	41.47701	-81.6824	benzene
OH	390350068	41.45478	-81.6344	benzene
OH	390350069	41.519	-81.6378	benzene
OH	390350071	41.49251	-81.67	benzene
OH	390490034	40.00274	-82.9944	benzene
OH	390515502	41.55002	-84.1365	benzene
OH	390610014	39.19433	-84.479	benzene
OH	390610044	39.13837	-84.7116	benzene

OH	390610045	39.17093	-84.5287	benzene
OH	390610046	39.11412	-84.5363	benzene
OH	390810017	40.36644	-80.6156	benzene
Ironton, OH	390875503	38.51814	-82.6688	PAHs, benzene
Franklin Furnace, OH	391450020	38.60934	-82.8225	PAHs, benzene
Franklin Furnace, OH	391450021	38.60066	-82.8296	PAHs, benzene
Franklin Furnace, OH	391450022	38.58808	-82.8348	PAHs, benzene
Warren, OH	391555504	41.23506	-80.8127	PAHs, benzene
MI	260330901	46.49361	-84.3642	benzene
MI	261110951	43.60917	-84.2106	benzene
MI	261110953	43.59139	-84.2094	benzene
MI	261110955	43.58944	-84.2211	benzene
MI	261110959	43.57419	-84.3216	benzene
MI	261630015	42.30279	-83.1065	benzene
Dearborn, MI	261630033	42.30754	-83.1496	PAHs, benzene
MI	261635502	42.35059	-83.0524	benzene
Liberty, PA	420030064	40.32377	-79.8681	PAHs, benzene
Clairton, PA	420033007	40.29434	-79.8853	PAHs, benzene
Kennedy Township, PA	420035503	40.49435	-80.0964	PAHs, benzene
PA	420450002	39.83556	-75.3725	benzene
PA	420710007	40.04667	-76.2833	benzene
PA	420770004	40.61194	-75.4325	benzene
PA	420910005	40.19255	-75.4575	benzene
PA	421010004	40.00889	-75.0978	benzene
PA	421010014	40.04962	-75.2408	benzene
PA	421010047	39.94465	-75.1652	benzene
PA	421010055	39.92287	-75.1869	benzene
PA	421010063	39.88294	-75.2197	benzene
PA	421010136	39.9275	-75.2228	benzene
PA	421190001	40.95517	-76.8819	benzene
PA	421250005	40.14667	-79.9022	benzene
PA	420010001	39.92002	-77.3097	benzene
PA	420030031	40.44337	-79.9903	benzene
Philadelphia, PA	421010449	39.9825	-75.0831	PAHs
Buffalo, NY	360291013	42.98844	-78.9186	PAHs, benzene
Rochester, NY	360551007	43.1462	-77.5481	PAHs, benzene
NY	360050133	40.8679	-73.8781	benzene
NY	360095501	42.08506	-78.4336	benzene
NY	360291007	42.7273	-78.8498	benzene
NY	360291014	42.99813	-78.8993	benzene
NY	360310003	44.39308	-73.8589	benzene
NY	360470118	40.69545	-73.9277	benzene

NY	360610115	43.84955	-79.9357	benzene
NY	360632008	43.08218	-79.0011	benzene
NY	360810124	40.73614	-73.8216	benzene
NY	360831003	42.73194	-73.6891	benzene
NY	360850111	40.58027	-74.1983	benzene
NY	360850132	40.58056	-74.1518	benzene
NY	361030009	40.82799	-73.0575	benzene
New York, NY	360050110	40.81616	-73.9021	PAHs, benzene
CT	90019003	41.11833	-73.3367	benzene
CT	90031003	41.78472	-72.6317	benzene
CT	90090027	41.3014	-72.9029	benzene
DE	100031008	39.5778	-75.6107	benzene
DE	100032004	39.73944	-75.5581	benzene
NJ	340155501	39.83709	-75.244	benzene
NJ	340210005	40.28309	-74.7427	benzene
NJ	340230006	40.47282	-74.4224	benzene
NJ	340230011	40.46218	-74.4294	benzene
NJ	340273001	40.78763	-74.6763	benzene
NJ	340390004	40.64144	-74.2084	benzene
NJ	340395502	40.65205	-74.1999	benzene
MD	240053001	39.31083	-76.4744	benzene
MD	240330030	39.05528	-76.8783	benzene
MD	245100006	39.34056	-76.5822	benzene
MD	245100040	39.29806	-76.6047	benzene
Washington, DC	110010043	38.92185	-77.0132	PAHs, benzene
Providence, RI	440070022	41.80795	-71.415	PAHs, benzene
RI	440030002	41.61524	-71.72	benzene
RI	440070026	41.87467	-71.38	benzene
RI	440071010	41.84157	-71.3608	benzene
NH	330110020	42.99578	-71.4625	benzene
NH	330111011	42.71866	-71.5224	benzene
NH	330115001	42.86175	-71.8784	benzene
NH	330150014	43.07533	-70.748	benzene
MA	250092006	42.47464	-70.9708	benzene
MA	250130008	42.19438	-72.5551	benzene
MA	250213003	42.21177	-71.114	benzene
MA	250250041	42.31737	-70.9684	benzene
Boston, MA	250250042	42.32944	-71.0825	PAHs, benzene
Northbrook, IL	170314201	42.14	-87.7992	PAHs, benzene
O'Hare airport, Chicago, IL	170313103	41.96519	-87.8763	benzene
Underhill, VT	500070007	44.52839	-72.8688	PAHs, benzene
VT	500070014	44.4762	-73.2106	benzene

VT	500210002	43.60806	-72.9828	benzene
East Chicago, IN	180895503	41.64921	-87.4475	PAHs, benzene
Gary, IN	180895504	41.5997	-87.3443	PAHs, benzene
IN	180190009	38.27668	-85.7638	benzene
IN	180855502	41.23898	-85.8321	benzene
IN	180890022	41.60668	-87.3047	benzene
IN	180890023	41.65274	-87.4396	benzene
IN	180890030	41.6814	-87.4947	benzene
IN	180970078	39.8111	-86.1145	benzene
IN	180970084	39.75885	-86.1154	benzene
IN	181270024	41.61756	-87.1993	benzene
IN	181570008	40.43164	-86.8525	benzene
IN	181630016	37.97444	-87.5323	benzene
Follansbee, WV	540095501	40.33564	-80.5953	PAHs, benzene
WV	540390010	38.3456	-81.6283	benzene
WV	540610003	39.64937	-79.9209	benzene
WV	540690010	40.11488	-80.701	benzene
Richmond, VA	510870014	37.55655	-77.4004	PAHs, benzene
VA	510330001	38.20087	-77.3774	benzene
VA	510590030	38.77335	-77.1047	benzene
VA	516700010	37.28962	-77.2918	benzene
VA	518100008	36.84188	-76.1812	benzene
OH	391450020	38.60934	-82.82251	N/A
OH	391450021	38.60066	-82.82964	N/A

B: Gas-particle partitioning analysis

B.1 Justification for exclusion of Junge-Pankow partitioning from GEM-MACH-PAH

Junge-Pankow partitioning (JP) is based on Langmuir adsorption (Langmuir, 1918). It expresses partitioning as a particulate fraction ϕ_k for each PAH species, k:

$$\phi_k = \frac{c\theta}{p^o_{L,k}+c\theta} \quad , \tag{B.1.1}$$

where ϕ_k is equal to the particulate concentration divided the total PAH species concentration. When ϕ_k =1, all of the concentration is in the particle phase, and none is in the gas phase, while ϕ_k =0 means all of the PAH is in the gas phase. θ is the total dry aerosol-particle surface area (m^2), $p_{L,k}^o$ is the subcooled liquid saturated vapor pressure per PAH species, and c is a constant that depends on the chemical species and the temperature (Junge, 1977).

The vapor pressure is calculated using the relation:

$$logK_{p,k} = m_K logp^o_{L,k} + b_K \tag{B.1.2}$$

where $m_{p,k}$ and $b_{p,k}$ come from Offenberg and Baker (1999)'s supporting information for PAHs.

Figure B.1b shows sample plots of ϕ_k vs log $p_{L,k}{}^o$. These examples show how the measurements (blue crosses) differ from the JP model (purple points and black line), which requires that m_K = -1 (see next section for the derivation of this). The JP formulation does not allow for improvement given the m_K = -1 constraint. Therefore, the Dachs-Eisenreich formulation is examined next.

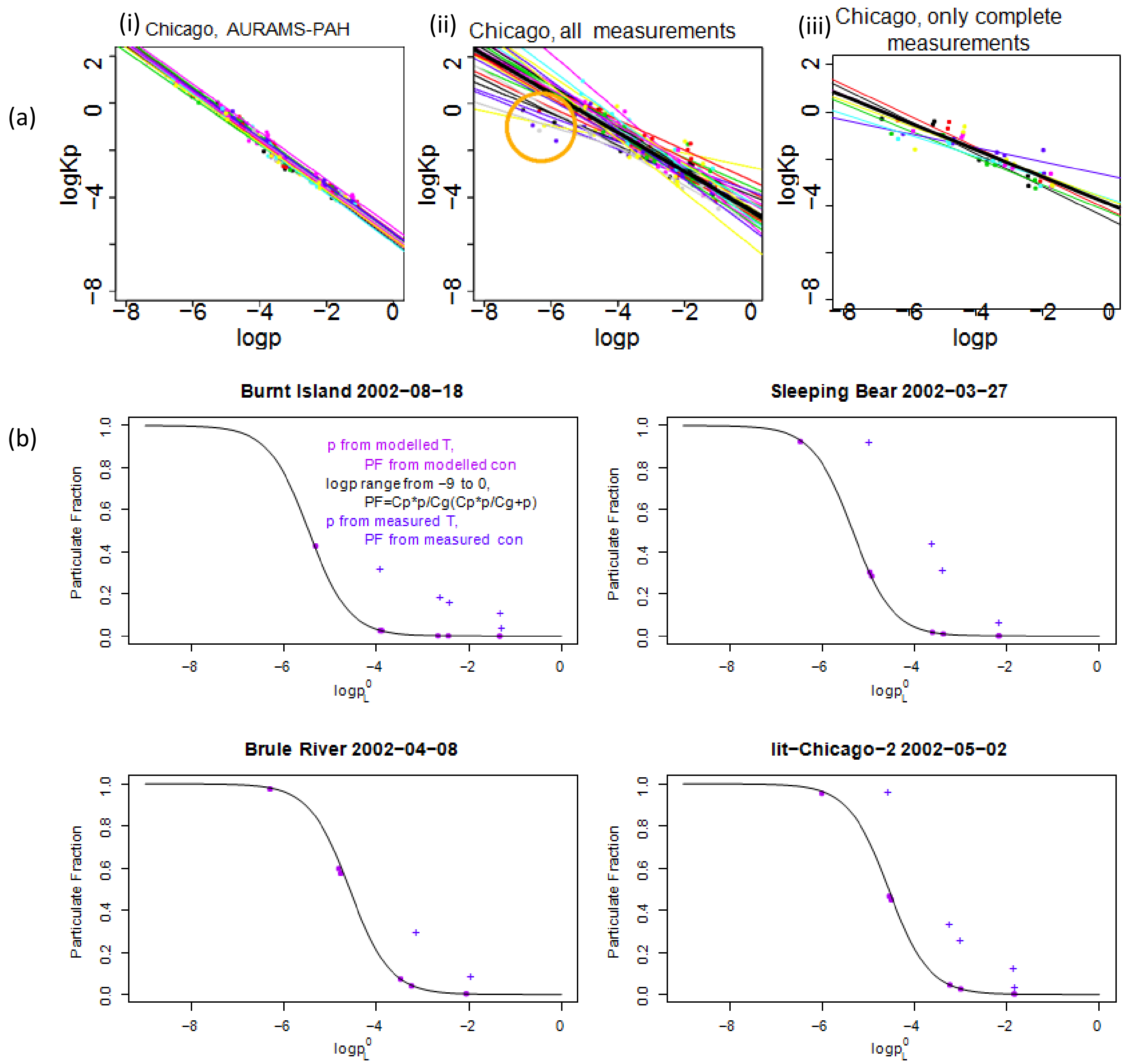

Figure B.1: (a) Chicago (taken as example) modelled (from AURAMS-PAH) and measured logKp vs logp° for all 7 PAHs, and their linear fits for 2002 data. Thick black line indicates the median linear fit. a(i) original JP and DE partitioning scheme, a(ii) all measurements, a(iii): only those measurements where all 7 PAHs were measured. (b) Particulate fraction (ϕ) vs logp_L^{o} for AURAMS-PAH model and 2002 measurement samples from four sites. The Junge-Pankow model is shown for 7 PAH species in purple points, and Eq. (B.1.1) as a black line. The measurements are shown as blue crosses.

B: Derivation of m = -1 for JP formulation, starting with Eq. (B.1.1)

Junge-Pankow relationship:

$$\phi = \frac{C_p}{C_p + C_g} = \frac{c\theta}{c\theta + p_L^\circ} \quad \text{(B1)}$$

$$\frac{C_p + C_g}{C_p} = \frac{c\theta + p_L^\circ}{c\theta} \quad \text{(B2)}$$

$$1 + \frac{C_g}{C_p} = 1 + \frac{p_L^\circ}{c\theta} \quad \text{(B3)}$$

$$\frac{C_g}{C_p} = \frac{p_L^\circ}{c\theta} \quad \text{(B4)}$$

$$\frac{C_p}{C_g} = \frac{c\theta}{p_L^\circ} \quad \text{(B5)}$$

(B6)

But,

$$\theta = C_{SSA}(\frac{m^2}{\mu g})C_{TSP}(\frac{\mu g}{m^3}) \quad \text{(B7)}$$

Subbing in:

$$\frac{C_p}{C_g} = \frac{cC_{SSA}C_{TSP}}{p_L^\circ} \quad \text{(B8)}$$

$$\frac{C_p/C_{TSP}}{C_g} = K_p = \frac{cC_{SSA}}{p_L^\circ} \quad \text{(B9)}$$

(B10)

Take log of both sides:

$$\log\left(\frac{C_p/C_{TSP}}{C_g}\right) = \log(cC_{SSA}) - \log(p_L^\circ) \quad \text{(B11)}$$

$$= -1\log(p_L^\circ) + \log(cC_{SSA}) \quad \text{(B12)}$$

Thus, for JP to be in a format that fits $\log K_p$ = m$\log p_L^\circ$ + b, m can only be -1.

B.2: Derivation of improved physico-chemical parameters for use with Dachs-Eisenreich partitioning

The Dach-Eisenreich expression for Kp is:

$$\begin{aligned} K_{p,k} &= 10^{-12}\left(\frac{1.5 f_{OC}}{\rho_{oct}} K_{OA,k} + f_{EC} K_{SA,k}\right) \\ &= 10^{-12} f_{EC} K_{SA,k} + 1.5 \times 10^{-12} \frac{f_{OC}}{\rho_{oct}} K_{OA,k} \end{aligned} \quad \text{(B.2.1)}$$

where f_{OC} and f_{EC} are the organic and elemental carbon fractions respectively, the 1.5 factor is an estimate to convert organic carbon to orgamic material, ρ_{oct} is the density of octanol, the octanol-air partitioning coefficient, $K_{OA,k}$, is related to temperature:

$$K_{OA,k} = 10^{\frac{m_{OA,k}}{T} + b_{OA,k}} \quad \text{(B.2.2)}$$

where $m_{OA,k}$ and $b_{OA,k}$ are taken from Odabasi et al (2006), and the soot-air partitioning coefficient, $K_{SA,k}$, is related to the soot-water and air-water partitioning coefficients:

$$\begin{aligned} K_{SA,k} &= K_{SW,k} e^{-K_{AW.k}} \\ &= K_{SW,k} e^{-(\frac{m_{AW,k}}{T} + b_{AW,k})}, \end{aligned} \quad \text{(B.2.3)}$$

where $m_{AW,k}$ and $b_{AW,k}$ are from Sander (1999) and Bamford et al (1999). An update for $b_{AW,k}$ was calculated from the 25^{o}C $K_{AW,k}$, values given in Ma et al (2010) using Eq. (B.2.3). $K_{OA,k}$ and ρ_{oct} are also well-known, and make the second term in Eq. (B.2.1) four orders of magnitude smaller than the first term. The $K_{SW,k}$ values (in Eq. (B.2.3)) are highly uncertain. Using our new AURAMS-PAH model-measurement comparisons, we have determined new $K_{SW,k}$ values that would improve the DE particulate fraction representation.

Fig. B.1a shows log$K_{p,k}$ vs log$p_{L,k}$ for each 2002 Chicago measurement sample (of multiple PAH species) in the Galarneau et al (2014) study (these are measurements of up to 7 PAH species in the gas and particle phases, thus for each PAH, the gas-particle partitioning coefficient (K_p can be plotted against that PAH's vapour pressure), and their linear fits. Eq. (B.1.2) governs the data relationship, but the observations have more spread in slope than the AURAMS-PAH model is capable of representing (shown in Figure B.1a). Using the JP or DE formulation, the model can not represent the variability in the slope, however, unlike the JP formulation, the DE model slope (m_K) *can* be altered to better match observations. The modeled slope, at -1, was too steep compared to the measurements (Fig. B.1a (i) vs. (ii) and (iii)). Note that most of the measured samples did not have BaP measurements, as this species is difficult to measure unless its concentrations are high. Therefore, the median line from the fits that include all samples (thick black line in Fig. B.1a(ii)) does not represent BaP measurements well. BaP points tend to fall well below the median line (see circle in Fig. B.1a(ii)). Therefore, we selected only samples that had all seven PAHs measured (from all sites -- shown in Fig. B.1a(iii) for Chicago samples), and calculated a median line from these linear fits. This median line better represents the slope and intercept of all PAHs, including BaP. Chicago was shown as an example, however, the original modelled slopes for all sites were too steep (too negative), and the intercepts too low.

Therefore, to adjust $K_{SW,k}$, we utilize the median m_k and b_k from the 2002 North American measurements, described above. First, we substitute Eq. (B.1.2) into Eq. (1) to get:

$$\log K_{p,k} = m_K\left(\frac{m_{p,k}}{T} + b_{p,k}\right) + b_K$$
$$= \frac{m_K m_{p,k}}{T} + m_K b_{p,k} + b_K \qquad \text{(B.2.4)}$$

Fig. 2a shows the all-site (2002) ensemble of AURAMS-PAH model-over-measured logK_p and (b) particulate fraction, in green. The `` adjusted model'' -- which is a actually just a re-calculation of logK_p from Eq. (B.2.4), using AURAMS-PAH temperature and the median measured m_K and b_K – is plotted in purple.

We then substitute Eq. (B.2.3) into Eq. (B.2.1), dropping the second term in equation (B.2.1) because we have verified that it is negligible, and because doing so greatly simplifies the math, to get:

$$K_{p,k} = 10^{-12} f_{EC} K_{SW,k} e^{-\left(\frac{m_{AW,k}}{T} + b_{AW,k}\right)} \qquad \text{(B.2.5)}$$

We set the right-hand-side of Eq. (B.2.4) equal to the log of $K_{p,k}$ from Eq. (B.2.5) to get our new $K_{SW,k}$ expression:

$$K_{SW,k} = \frac{10^{\left(\frac{m_K m_{p,k}}{T} + m_K b_{p,k} + b_K + 12\right)}}{f_{EC} e^{-\left(\frac{m_{AW,k}}{T} + b_{AW,k}\right)}} \qquad \text{(B.2.6)}$$

Eq. (B.2.6) is thus a means of describing PAH partitioning based on measurements, and the resulting $K_{SW,k}$ values are summarized in Table 1. The new $K_{SW,k}$ values will go into equation B.2.3 to give new $K_{SA,k}$ values that will go into equation B.2.1, which does the PAH partitioning in the model.

C: Description of mobile source emission factors for PAHs from the literature and SPECIATE

We require total PAH (gas + particle phases) emissions for our model, however about half of the compiled EFs (from the literature and from SPECIATE) only reported EFs for the particulate component of total PAH. Therefore, the EFs from those studies were not used. The remaining SPECIATE data contained values that were sometimes unrealistically high (e.g., up to 20% phenanthrene in the TOG mass, which is orders of magnitude larger than typical values), and the relevant databases and reports lacked explanations for these anomalies. Therefore, none of the SPECIATE EFs were used in our determination of new PAH emissions.

From the remaining publications, the on-road EFs we recorded fell into the following eight vehicle categories (e.g., LDGV (Lim et al., 2007; de Abrantes et al., 2009); LDDV (Karavalakis et al., 2011); LDDT (Westerholm et al., 2001; Nelson et al., 2008); HDDV (Mi et al., 2000; Lim et al., 2005; Nelson et al., 2008); and MC (Yang et al., 2005; Spezzano et al., 2008)). When the EFs were converted to units of mass PAH per mass TOG for each of the vehicle classes, it was found that for some species/vehicle classes the EFs spanned up to two orders of magnitude within the same study, and up to three orders of magnitude across different studies. The EFs differ greatly within each category because the studies examined report on emissions from a variety of fuels (e.g., diesel can have varying percentages of biodiesel added), driving speeds (e.g., idling, city driving, highway driving, etc), and temperatures (e.g., cold start, cold outdoor temperatures, warm engine, etc.), whereas the TOG values that the PAHs were normalized to were only reported for different types of roads (e.g., urban, highway). When publications reported EFs for multiple fuel types, the most relevant EFs were kept (e.g., in Canada only ultralow sulfur diesel (ULSD), and unleaded gasoline fuels are used).

With these updated PAH EFs in hand, SMOKE was run to generate gridded emissions files of 28 usual GEM-MACH emitted species plus benzene and seven gas-phase PAHs on two model grids, a continental grid with 10-km horizontal grid spacing (Fig. 1a) and the “Pan Am” grid with 2.5-km grid spacing (Fig. 1b). We then ran the model with both the ``recent-literature-based'' EFs for eight vehicle classes (using the median value in each category) and with MOVES 2014 EFs for just two classes (gasoline and diesel). The literature based EFs were generally higher than those from MOVES. The model biases for PAHs were smaller with the MOVES EFs in both Canada and the U.S., therefore, the model results we show in Section 4 are from the simulation with MOVES mobile emissions. We will discuss the results of the on-road mobile EFs further when we analyze the model output (Section 4.2.1).

D: Table of species-specific constants used in the model for dry and wet removal.

Table D.1: Species-specific constants used in the model for dry and wet scavenging.

Constant	Benzene	PHEN	ANTH	FLRT	PYR	BaA	CHRY	BaP	Source
[1] α	0.05	0.1	0.1	0.2	0.2	0.2	0.2	0.3	Zhang et al (2015)
[2] β	0.1	0.3	0.3	0.4	0.4	0.5	0.5	0.6	Zhang et al (2015)
[3] H* (unit)	22.7	22.7	20.2	70.1	76.8	146	227	91.1	Staudinger & Roberts (2001) for benzene. Ma et al. (2010) for PAHs
[4] f_0 (unit)	0	0	0	0	0	0	0	0	NA
[5] ats (K)	3950	4700	4000	6900	6900	4700	4700	2405	Sander (1999)
[6] vap. pres. slope	-1211.03	-3706.04	-3710.87	-4081.11	-4153.89	-4563.27	-4577.21	-5046.88	Shiu and Ma (2000)
[7] vap. pres. Int.	6.0299	11.42	11.42	11.59	11.62	11.81	11.82	12.04	Shiu and Ma (2000)

[1]weights applied to resistance for SO_2 for a given gas

[2]weights applied to resistance for O_3 for a given gas

[3]Henry's law constant, solubility in water

[4]chemical reactivity, used to evaluate how much gas is dissolved in mesophyll

[5]temperature dependency for solubility

[6]sub-cooled liquid satureation vapour pressure (Pa), slope

[7]sub-cooled liquid satureation vapour pressure (Pa), intercept

E: Hamilton $PAH_i/PM_{2.5}$ analysis

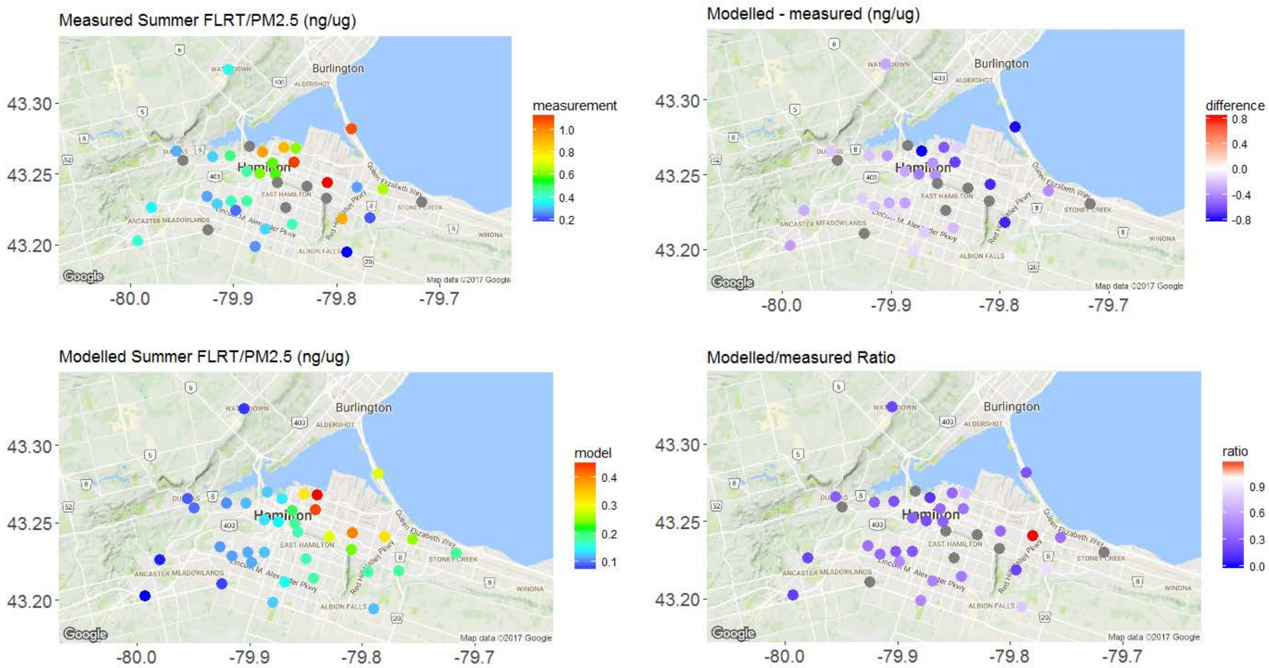

Figure E.1: Left: Measured and modelled and concentration ratios of $FLRT/PM_{2.5}$ in Hamilton, Ontario for two-week summer 2009 period. Right: Their differences and ratios. Note that spatial pattern in model bias is missing.

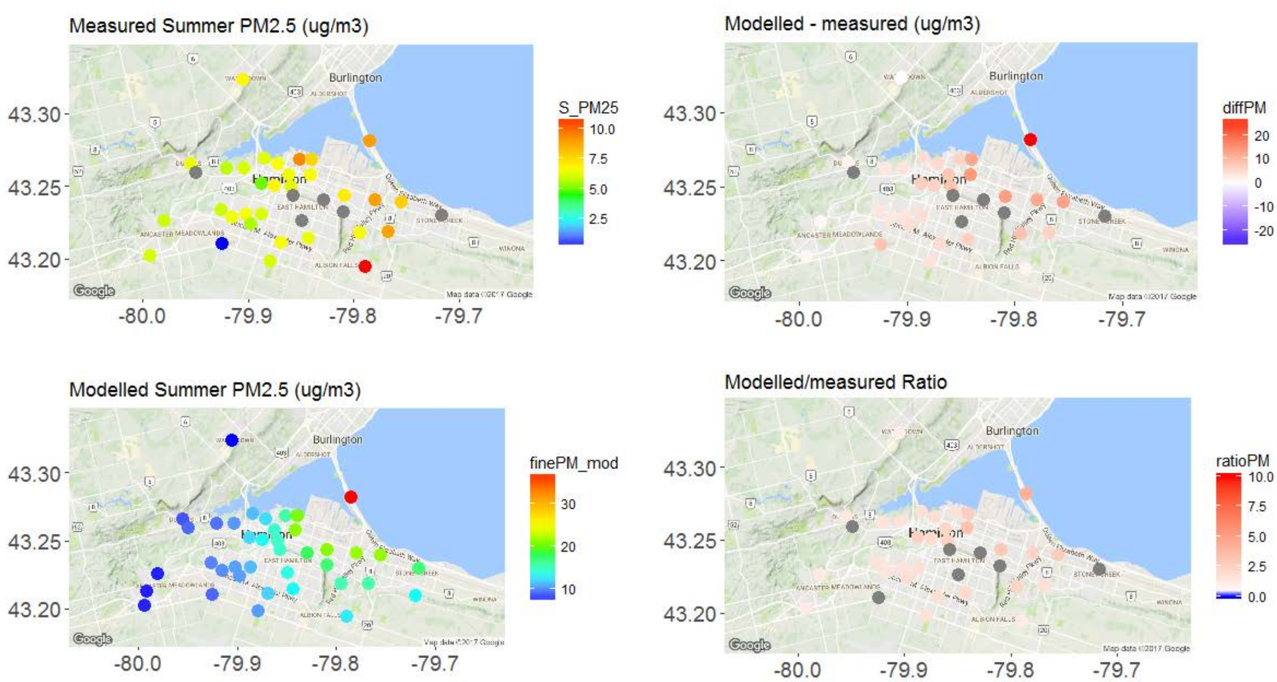

Figure E.2: Same as Fig. E.1, but for $PM_{2.5}$ concentrations. Note that modelled $PM_{2.5}$ is biased high, and is causing the spatial pattern seen in the PAH bias (cf. Fig. 4a).

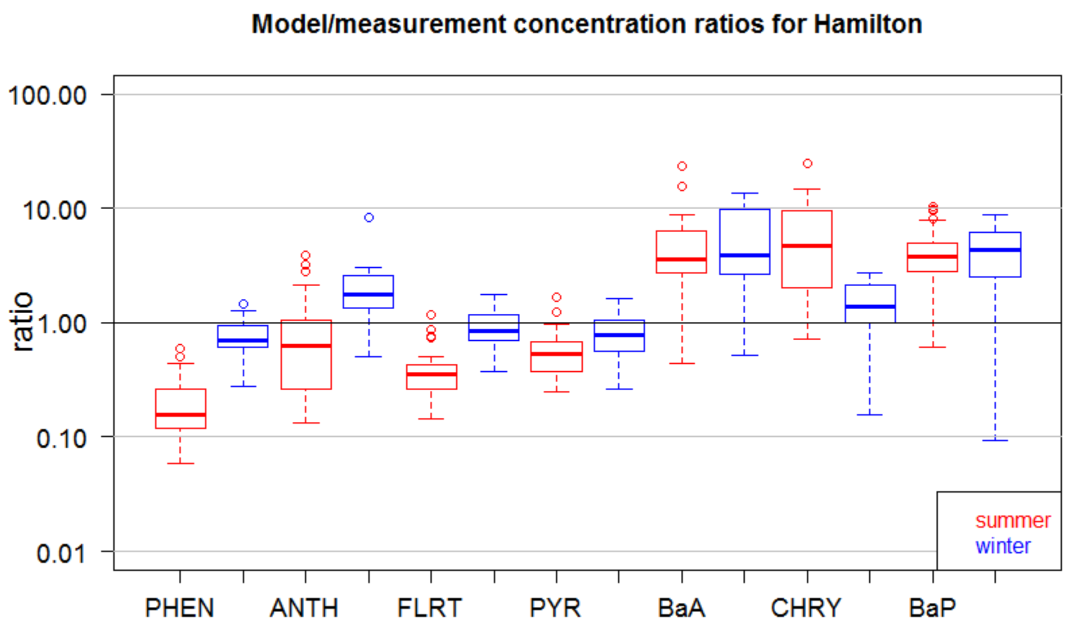

Figure E.3: Model/measurement ratios of $PAH_i/PM_{2.5}$ in Hamilton (summer and winter). Note that all biases have shifted down compared to Fig. 5a because the modelled $PM_{2.5}$ is biased high compared to measurements.

References

Bamford, H. A., Poster, D. L., and Baker, J. E.: Temperature dependence of Henry's Law constants of thirteen polycyclic aromatic hydrocarbons between 4°C and 31°C, Environ. Toxic. Chem., 18, 1905–1912, 1999.

de Abrantes, R., de Assunção, J. V., Pesquero, C. R., Bruns, R. E., and Nóbrega, R. P.: Emission of polycyclic aromatic hydrocarbons from gasohol and ethanol vehicles, Atmos. Environ., 43, 648–654, doi:10.1016/j.atmosenv.2008.10.014, 2009.

Galarneau, E., Makar, P. A., Zheng, Q., Narayan, J., Zhang, J., Moran, M. D., Bari, M. A., Pathela, S., Chen, A., and Chlumsky, R.: PAH concentrations simulated wit hthe AURAMS-PAH chemical transport model over Canada and the USA, Atmos. Chem. Phys., 14, 4065–4077, doi:10.5194/acp-14-4065-2014, 2014.

Junge, C. E.: Basic considerations about trace constituents in the atmosphere as related to the fate of global pollutants, in: Fate of pollutants in the air and water environments, edited by Suffet, I. H., pp. 7–25, Wiley, New York, 1977.

Karavalakis, G., Boutsika, V., Stournas, S., and Bakeas, E.: Biodiesel emissions profile in modern diesel vehicles. Part 2: Effect of biodiesel origin on cabonyl, PAH, nitro-PAH and oxy-PAH emissions, Sci. Tot. Environ., 409, 738–747, doi:10.1016/j.scitotenv.2010.11.010, 2011.

Langmuir, I.: The adsorption of gases on plane surfaces of glass, mica, and platinum, J. Am. Chem. Soc., 40, 1361–1402, 1918.

Lim, M. C. H., Ayoko, G. A., Morawaska, L., Ristovski, Z. D., and Jayaratne, E. R.: Effect of fuel composition and engine operating conditions on polycyclic aromatic hydrocarbon emissions from a fleet of heavy-duty diesel buses, Atmos. Environ., 39, 7836–7848, doi:10.1016/j.atmosenv.2005.09.019, 2005.

Lim, M. C. H., Ayoko, G. A., Morawaska, L., Ristovski, Z. D., and Jayaratne, E. R.: Influence of fuel composition on polycyclic aromatic hydrocarbon emissions from a fleet of in-service passenger cars, Atmos. Environ., 41, 150–160, doi:10.1016/j.atmosenv.2006.07.044, 2007.

Ma, Y.-G., Lei, Y. D., Xiao, H., Wania, F., and Wang, W.-H.: Critical review and recommended values for the physical-chemical property data of 15 polycyclic aromatic hydrocarbons at 25°C, J. Chem. Eng. Data, 55, 819–825, doi:10.1021/je900477x, 2010.

Mi, H.-H., Lee, W.-J., Chen, C.-B., Yang, H.-H., and Wu, S.-J.: Effect of fuel aromatic content on PAH emission from a heavy-duty diesel engine, Chemosphere, 41, 1783–1790, 2000.

Nelson, P. F., Tibbett, A. R., and Day, S. J.: Effects of vehicle type and fuel quality on real world toxic emissions from diesel vehicles, Atmos. Environ., 42, 5291–5303, doi:10.1016/j.atmosenv.2008.02.049, 2008.

Odabasi, M., Cetin, E., and Sofuoglu, A.: Determination of octanol-air partition coefficients and supercooled liquid vapor pressures of PAHs as a function of temperature: application to gas-particle partitioning in an urban atmosphere, Atmos. Environ., 40, 6615–6625, doi:10.1016/j.atmosenv.2006.05.051, 2006.

Offenberg, J. H. and Baker, J. E.: Aerosol size distributions of polycyclic aromatic hydrocarbons in urban and over-water atmospheres, Environ. Sci. Technol., 33, 3324–3331, doi:10.1021/es990089c, 1999.

Sander, R.: Modeling atmospheric chemistry: interactions between gas-phase species and liquid cloud/aerosol particles, Surveys in Geophysics, 20, 1–31, 1999.

Shiu, W.-Y., Ma, K.-C.: Temperature dependence of physical-chemical properties of selected chemicals of environmental interest. I. Mononuclear and polynuclear aromatic hydrocarbons, J. Phys. Chem. Ref. Data, 29, no. 1, 41-130, doi:10.1063/1.556055, 2000.

Spezzano, P., Picini, P., Cataldi, D., Messale, F., and Manni, C.: Particle- and gas-phase emissions of polycyclic aromatic hydrocarbons from two-stroke, 50-cm3 mopeds, Atmos. Environ., 42, 4332–4344, doi:10.1016/j.atmosenv.2008.01.008, 2008.

Staudinger, J., Roberts, P. V.: A critical compilation of Henry’s law constant temperature dependence relations for organic compounds, Chemosphere, 44, 561-576, doi:10.1016/S0045-6535(00)00505-1, 2001.

Westerholm, R., Christensen, A., Törnqvist, M., Ehrenberg, L., Rannug, U., Sjögren, M., Rafter, J., Soontjens, C., Almén, J., and Grägg, K.: Comparison of exhaust emissions from Swedish environmental classified diesel fuel (MK1) and European program on emissions, fuels, and engine technologies (EPEFE) Reference fuel: a chemical and biological characterization, with viewpoints on cancer risk, Environ. Sci. Technol., 35, 1748–1754, doi:10.1021/es000113i, 2001.

Yang, H.-H., Chien, S.-M., Chao, M.-R., and Lin, C.-C.: Particle size distribution of polycyclic aromatic hydrocarbons in motorcycle exhaust emissions, J. Haz. Mat., B125, 154–159, doi:10.1016/j.jhazmat.2005.05.019, 2005.

Zhang, L., Cheng, I., Muir, D., Charland, J.-P.: Scavenging ratios of polycyclic aromatic compounds in rain and snow in the Athabasca oil sands region, Atmos. Chem. Phys., 15, 1421-1434, doi: 10.5194/acp-15-1421-2015, 2015.